C. R. Physique 19 (2018) 641–656

Contents lists available at ScienceDirect

Comptes Rendus Physique

www.sciencedirect.com

New trends in metallic alloys / Alliages métalliques : nouvelles tendances

New developments of advanced high-strength steels for automotive applications

Nouveaux développements dans le domaine des aciers à très haute résistance pour les applications automobiles

Jean-Hubert Schmitt [a,*], Thierry Iung [b]

[a] *MSSMat, CNRS, Centrale Supélec, Université Paris-Saclay, 91190 Gif-sur-Yvette, France*
[b] *ArcelorMittal Global R&D – Maizières, Voie Romaine, 57283 Maizières-lès-Metz, France*

ARTICLE INFO

Article history:
Available online 28 November 2018

Keywords:
Advanced high-strength steels
TRIP steels
TWIP steels
Q&P steels
Medium-Mn steels
Automotive applications

Mots-clés :
Aciers à très haute résistance
Aciers TRIP
Aciers TWIP
Procédé Q&P
Aciers moyen Mn
Application automobile

ABSTRACT

Automotive industry asks for higher resistant steels to lighten parts and improve crash resistance. Keeping a good ductility while increasing tensile strength requires the development of new grades in which hardening mechanisms counteract the drop in elongation when enhancing mechanical resistance. This is mainly achieved with multiphase steels and completing dislocation hardening by twinning and martensite transformation during straining. This has led to high-strength steel families, some of them being already used in body in white (Dual Phase (DP) and TRIP steels). Others, still in development, will soon emerge on the market (Quenched and Partitioned (Q&P), medium-Mn steels or TWIP).

RÉSUMÉ

L'industrie automobile demande des aciers plus résistants pour alléger les pièces et améliorer la résistance aux chocs. Le maintien d'une bonne ductilité tout en augmentant la résistance à la traction nécessite le développement de nouvelles nuances dans lesquelles les mécanismes de durcissement compensent la baisse de l'allongement en augmentant la résistance mécanique. Ceci est principalement réalisé avec des aciers multiphasés et en complétant le durcissement par dislocation par du maclage et une transformation martensitique pendant la déformation. Ceci a donné naissance à des familles d'aciers à haute résistance dont certaines sont déjà utilisées pour la caisse en blanc (aciers Dual Phase (DP) et TRIP). D'autres, encore en cours de développement, apparaîtront bientôt sur le marché (aciers trempés et partitionnés (Q&P), aciers à moyenne teneur en manganèse ou TWIP).

* Corresponding author.
E-mail address: jean-hubert.schmitt@centralesupelec.fr (J.-H. Schmitt).

https://doi.org/10.1016/j.crhy.2018.11.004

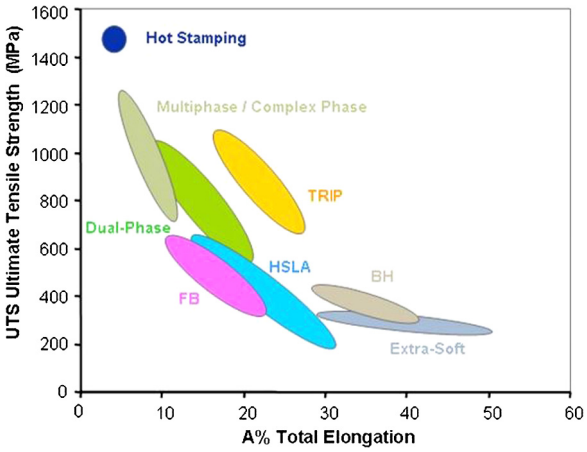

Fig. 1. Representation of the main low-alloyed steel grades in the UTS vs. total elongation diagram. Dual-phase, TRIP, complex phase, and hot stamping steels are considered the first generation of high-strength steels.

1. Introduction

The development of materials for automobile applications, especially for the body in white, results from multiple and often contradictory constraints: a search for lightness, a high formability to satisfy the needs of renewed external designs, a sufficient stiffness for vehicle handling, a high mechanical strength for safety reasons, production possibilities in large quantities with a high productivity, a great ease of assembly, a durable surface in a severe environment maintaining excellent aesthetic properties, all under strong economic constraints. If the resolution of contradictory objectives is frequently the task of the metallurgist, such a combination for steel, a material deemed so well known, remains a real challenge.

One of the first problems is to combine an excellent formability with a high mechanical strength, two largely antagonistic properties, at least as long as only a single hardening mechanism is operating. It results from the well-known Considère criterion in tension [1] and is clearly illustrated by the total elongation *vs*. tensile strength (UTS) diagram on which different steel grades are represented (Fig. 1). In the 1980s, part of this difficulty was circumvented by separating the two requirements with a design solution: a resistant mesh structure made of beams and pipes, on the one hand, and a thin skin for the visible parts, on another hand. This led to the development of very low-carbon interstitial free steels (IF) with low addition of titanium to precipitate residual carbon in ferrite, and even to ultra-low carbon steels (ULC) since secondary liquid metallurgy made it possible to reach carbon amounts below 10 ppm in weight. These steels are single-phase iron with a body-centered cubic (bcc) structure at room temperature, with carbon in interstitial solid solution, a phase named ferrite. These "extra-soft" grades, IF and ULC, have a yield stress of about 100 MPa, close to the one of pure iron, and a total elongation quite important (50%). They possess a very high formability compatible with the new complex shapes of body parts looked for by the automotive designers. This solution, however, gave opportunities for aluminum and polymer solutions for visible skin parts,[1] unsatisfactory for the steelmaker. It was therefore an outright necessity to create new steel grades that best combined mechanical strength and ductility, and, to do this, to get out of the only mechanism of work hardening by dislocations in ferrite.

Taking advantage of a phase transition in carbon steels, dual phase steels (DP steels) were developed. Hardening comes from a second hard phase, martensite, obtained from quenching at room temperature of the austenite, a face-centered cubic (fcc) phase that is stable at temperatures above 910 °C for pure iron. This steel grade represented the first generation of advanced high-strength steels (AHSS) with ultimate tensile strength (UTS) up to 1200 MPa and reasonable elongation around 10 to 15% (Fig. 1). The first part of this paper recalls the industrial development of these DP steels and some of their derivations into new AHSS grades still using the hardness of martensite.

New European regulations on CO_2 emission – 95 g/km CO_2 in 2020 and a target of 30% further reduction by 2030 – have been changing the game as they are now coupled with a financial penalty. Since weight lightening strongly impacts fuel consumption (10% weight reduction leads to fuel economy of 5.5% [2]), and so CO_2 emission [3], extra cost for the development of performant steel grades can now be valorized. Larger amounts of alloying elements can be used and more complex industrial processes implemented. It is opening the way for totally new metallurgies: carbon steels for hot stamping, austenitic carbon–manganese steels, AHSS duplex steels... These stepwise evolutions had given rise to new steel families known as the 2nd and 3rd generations of advanced high-strength steels.

This paper successively presents these evolutions, the key features of these new grades, the induced process constraints, and their possible evolutions.

[1] The most typical example in France was the first models in the Matra–Renault family called 'Espace', with a car body mostly composed of polymer matrix composite in 1983.

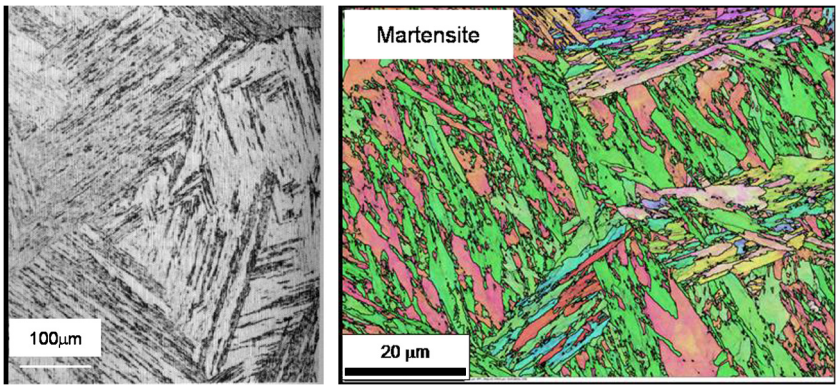

Fig. 2. Microstructure of a martensitic carbon steel (optical micrograph).

2. Hardening by martensitic microstructure

2.1. Metastable phases in carbon steel and hardening

When carbon steel is rapidly quenched from high temperature to a sufficiently low temperature, austenite has no time to transform into ferrite by diffusion. The transformation is said "displacive", and the fcc structure of the austenitic transforms into a quadratic mesh by shear and dilatation, the Bain transformation [4,5]. It leads to a complex microstructure, composed of fine laths or thin plates, sub-micrometric for the smallest dimension, supersaturated in carbon and containing a high density of dislocations (Fig. 2). The martensitic microstructure provides a very high yield stress that depends, in the first order, on the carbon amount. Since its mechanical behavior is not easy to predict, empirical formulae are frequently used to linearly correlate the yield stress and the ultimate tensile stress with the carbon content [4,6]. More recently, Allain et al. developed a continuous composite approach to account for the strain hardening of the martensite microstructure [7]. It results a relatively low ductility, characterized by a total elongation of a few percent, for a tensile strength up to 2000 MPa.

The fraction of martensite only depends on the final cooling temperature. The austenite starts to transform at a temperature M_s, which is a function of the carbon amount and the volume fraction of the alloying elements [8]:

$$M_s(°C) = 565 - 600\big(1 - \exp\big(-0.96[C]\big)\big) - 31[Mn] - 13[Si] - 10[Cr] - 8[Ni] - 12[Mo] \quad (1)$$

where $[X]$ is the amount of element X in wt.%. It is to be noted that any addition of alloying elements decreases the start temperature of transformation, carbon being the most influent element.

At a temperature above M_s and below a critical one M_d, also depending on the steel composition [9], an elastic stress or a plastic strain can destabilize austenite and induce a martensitic transformation [10,11]. This mechanism is known as transformation-induced plasticity (TRIP) [12]. Even though the influence of the different alloying element is not quantitatively the same on the values of M_s and M_d, it works in a similar way, that is, an addition of carbon, manganese, or nickel, for instance, favors the TRIP mechanism at room temperature.

2.2. DP and TRIP steels: a first industrial success story

In the end of the 1990s, an important worldwide program was launched by 35 steel companies from 18 countries to improve steel for body in white. The ULSAB program concluded an extensive use of high-strength steels, allowing a decrease in the weight of a four-door sedan by 25% at a lower cost of 10%. A second program (ULSAB-VAB) proved that the results could even be improved by using 80% of AHSS grades, mainly DP and TRIP steel sheets [3].

2.2.1. Dual-phase steels

Owing to a relatively simple process for quenching thin sheets to room temperature, DP steels were the first to be industrially produced. Their metallurgy was based on relatively ancient academic work [13,14] and on thick plate developments [15,16]. The challenge was a limitation of the alloying elements for the cost, and process improvement for a profitable production of homogeneous thin sheets on continuous lines.

A DP steel is usually composed by a ferrite matrix containing martensite islands. The volume fraction of martensite can be varied on a large scale from 10 to 50%. It is even possible to produce '*martensitic*' grades with nearly 100% of martensite; in this case, ferrite decorates martensite islands. To get such a microstructure, cold-rolled sheets with a ferrite–pearlite microstructure are annealed at a temperature within the intercritical range, where ferrite and austenite are in equilibrium (Fig. 3a). The annealing temperature is set up to control the volume fraction of martensite: the higher the temperature, the larger the austenite amount, and so the martensite amount after cooling. During the soaking time at the annealing temperature, carbon diffuses from ferrite to austenite according to the thermodynamic equilibrium. Sheets are then quenched to

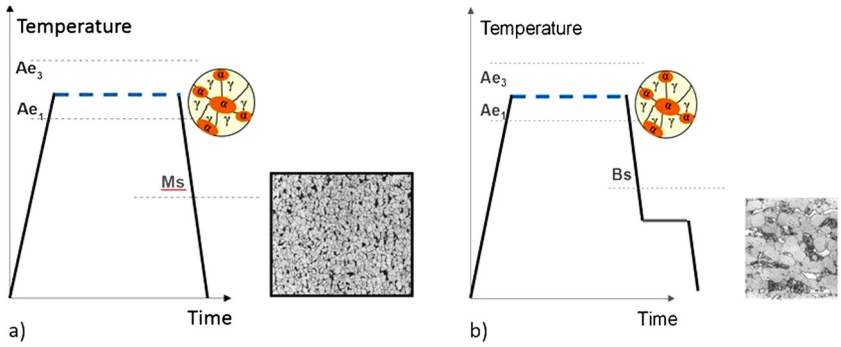

Fig. 3. Schematic schedule for the annealing process of DP (a) and TRIP steels (b).

room temperature, so the carbon-enriched austenite transforms into martensite. The heating rate is usually defined so that the cold-rolled microstructure recrystallizes and gives a fine final microstructure – about 5 µm ferritic grain size or less, and 1 µm for martensite – which increases the final strength of the alloy.

To insure good weldability, the carbon content must be kept as low as possible. Usually the carbon amount lies between 0.1 and 0.2 wt.%. The other main alloying elements are manganese (0.7 to 2 wt.%) and silicon (0.1 to 0.3 wt.%). The equilibrium between the two phases present at annealing temperature implies a relation between the volume fraction of austenite and the carbon amount within this phase. When the volume fraction of austenite is low (say between 10 and 20%), the carbon amount is as high as 0.6 wt.%. The resulting martensite is then very hard and its behavior during straining of a DP sample is mainly elastic. The mechanical behavior of these DP grades is mainly controlled by the volume fraction of martensite [17]. The UTS is high, as is work hardening (a fraction of the Young's modulus at low strain, between $E/50$ and $E/20$), which leads to a large uniform elongation (on the order of 15 to 20%) [18]. The yield stress, however, tends to be low, since the early stage of plasticity is mainly due to the ferrite matrix.

Conventional annealing lines are not actually adapted for the industrial production of DP steels. In fact, they are designed with an overaging step for some tenths to hundreds of seconds at a temperature between 300 and 500 °C to control the carbon in solid solution in ULC steels. For DP grades, such a temperature range corresponds to the bainitic transformation and alloying elements as Cr, Mo, or Mn would be necessary to avoid this constituent. So industrial production of DP steels was facilitated by the development of water-quenching industrial lines. As most of steels for the automotive industry is hot-dip coated in a liquid zinc bath at 460 °C after annealing, attention should be paid to the duration of this treatment, and the alloying elements must be adjusted in steel to suppress any possibility of bainite formation.

For some specific applications, as anti-intrusion beams, a high yield stress is expected. The volume fraction of martensite is increased and, at the limit, reaches almost 100%. But, consequently, the carbon amount in martensite is relatively low and approaches the nominal amount of the steel for martensitic grades. Martensite then exhibits an elastic–plastic behavior, with low hardening. It leads to an increase in the DP yield stress, since martensite forms a continuous skeleton for volume fractions above 30%. The uniform elongation is drastically reduced to a few percent [17]. A short tempering step can be added after quenching to limit the martensite brittleness.

The automotive market also demands DP steels for thicker parts, like wheels [19]. These parts are made with hot-rolled sheets. The dual-phase microstructure is obtained by controlling the rolling final temperature and the cooling rate. This is now possible thanks to the improvement of hot rolling mills and the development of instrumented cooling table. For other parts, stamped from thinner cold-rolled sheets, an optimum of the balance strength–elongation is obtained for DP grades with a martensitic volume fraction between 10 and 20% [3]. They give rise to a yield stress about 300–700 MPa, UTS from 600 MPa to above 1000 MPa, and uniform elongation larger than 10%.

Composite mechanical modeling, based on deformation physical mechanisms, have been developed, which helps and speeds up the metallurgical design of grades with foreseen mechanical properties [17].

2.2.2. TRIP steels

One of the limitations in developing ultra-high strength materials is the induced dramatic decrease of the uniform elongation (Fig. 1). To keep elongation uniform at the largest strains implies to increase work hardening. But it is physically well established that hardening by dislocation interactions as in ferrite is decreasing progressively as strain is increasing. As seen above (§ 2.2.1), adding a second phase gives an extra macroscopic work hardening coming from the elastic behavior of martensite. However, this effect is less and less important when straining progresses, and a final strong drop of work hardening in DP steels results from the elastic–plastic transition in the martensite behavior, associated with a subsequent low strain hardening [17]. To conclude, the possibility to improve ductility while increasing the maximum strength could result from a hardening mechanism by which work hardening does not saturate at large strain.

Such a mechanism was early identified in materials with unstable austenite that gradually transforms into martensite during straining (TRIP steels) [12]. A limitation for the industrial development of such grades was linked to the cost of the alloying elements needed to stabilize austenite at room temperature (Eq. (1)). This is the case, for instance, for unstable

austenitic AISI 301 stainless steel, which contains 0.1% carbon, 18% chromium, and 8% nickel (in wt.%) [20]. Lean stainless austenitic grades were more recently designed, in which manganese substitutes itself partly for the more expensive nickel as the addition element. AISI 201 grade exemplifies this trend, with an increase of the carbon amount up to 0.15 wt.% and addition of 5.5 to 7.5 wt.% manganese, which allows one to decrease the nickel amount below 5.5 to 3.5 wt.% [21].

The challenge was then to activate a same mechanism with a smaller amount of less expensive alloying elements, knowing that for DP steel composition, as seen above, austenite is not stable at room temperature. To save the welding properties, the chemical composition of low-carbon TRIP steels developed for the automotive industry is close to the one for DP: carbon amount between 0.2 and 0.25 wt.%, and a slight increase of manganese amount up to 2 wt.%. The main difference is the addition of more than 2 wt.% of aluminum and silicon [22]. The first part of the annealing process is identical as for DP steels. The soaking time and annealing temperature allow obtaining a duplex microstructure ferrite–austenite with typically a volume fraction of 50% of each phase. As already seen, the austenite carbon concentration in the range from 0.3 to 0.4 wt.% is not enough to stabilize austenite at room temperature. So, a second step was introduced in the annealing process: after quenching from the annealing temperature down to 300–350 °C to avoid any pearlite precipitation, the sheets were held at this temperature to let time for austenite to transform in low-carbon bainite [22] (Fig. 3b). This step advantageously corresponds to the overaging step in an industrial annealing line easing TRIP steel production. During phase transformation, carbon is rejected from bainite to untransformed austenite. Silicon and aluminum additions suppress carbide formation and carbon enrichment is maintained in residual austenite [23–25]. Sheets are then cooled down to room temperature, the carbon enrichment of austenite being enough to get a metastable phase, i.e. room temperature lies between M_s and M_d for the actual composition of austenite. It results a rather complex microstructure with about 50% of ferrite, 35 to 40% of bainite, and 10 to 15% of austenite. Very high-strength TRIP grades are now reaching a maximum tensile stress above 1200 MPa with a uniform elongation up to 14%.

The high elongation of these grades comes from a progressive martensitic transformation, which contributes to a complementary hardening of steel during straining. TRIP steel can be considered as a composite material with a soft phase (ferrite + bainite + austenite), whose constitutive law may be estimated from a multiphase approach [26], and a hard phase represented by martensite. In fact, this is even a “dynamic composite” as the volume fraction of the hard phase is not constant. Assuming that, at a first order, the work hardening of a two-phase material is expressed as [26,27]:

$$\frac{\mathrm{d}\sigma}{\mathrm{d}\varepsilon} = (1 - f_\mathrm{m})\frac{\mathrm{d}\sigma_\mathrm{M}}{\mathrm{d}\varepsilon_\mathrm{M}} + f_\mathrm{m}\frac{\mathrm{d}\sigma_\mathrm{m}}{\mathrm{d}\varepsilon_\mathrm{m}} + \frac{\mathrm{d}f_\mathrm{m}}{\mathrm{d}\varepsilon}(\sigma_\mathrm{m} - \sigma_\mathrm{M}) \tag{2}$$

f_m is the instantaneous volume fraction of martensite and σ, σ_M, and σ_m (resp. ε, ε_M, and ε_m) are the stress (resp. the strain) of the TRIP steel, the multiphase matrix and the martensite, respectively. The evolution of the martensite amount with respect to strain is [11]:

$$f_\mathrm{m} = 1 - \exp\left\{-\beta\left[1 - \exp(-\alpha\varepsilon)\right]^n\right\} \tag{3}$$

α is a parameter related to the number of shear bands in austenite through the stacking fault energy, β represents the probability of a martensite nucleus to form, assuming it forms at a shear band intersection, and n is an exponent considered as a material constant depending on the actual composition of the retained austenite.

At large strain, when the work hardening mainly due to dislocation interactions in ferrite, bainite and austenite tends to saturate, martensite transformation generates a complementary hardening with the extra-strength due to an increase of the martensite amount [28]. This is frequently seen on the stress–strain curves for which the slope is increasing when approaching necking (Fig. 4). This behavior is strongly linked to the kinetics of the martensite transformation [25,29,30]: when the transformation kinetics is too fast, the mechanical behavior rapidly approaches a DP behavior with a high UTS value, but a limited total elongation. On another hand, for a too slow kinetics, the tensile stress is moderate as well as strain hardening.

Due to the high uniform elongation, there is usually a possible residual “deformation capacity” after drawing. Coupled with the high stress resulting from work hardening, the mechanical energy for a subsequent deformation is then very important. This makes TRIP steel of great benefit for energy absorption, better in car crash situations compared with other AHSS grades (Fig. 5) [3].

2.3. High-strength steel for hot stamping

A limit for deep drawing of DP steels with a high volume fraction of martensite is their low ductility [17,26]. Such a problem is well known for highly resistant long products formed by cold forging, for instance. The common solution is to form the part with a rather soft microstructure, then to apply a thermal treatment to quench and harden the final part. Another advantage of hot forming is a strong reduction of the springback (i.e. part-shape evolution by elastic deformation after forming) after forming since the Young’s modulus is lower at higher temperature. The process has been evolving to combine the forming process and the thermal treatment in a single pass to save time and money. Based on this method, hot stamping of thin sheets was developed for saw blade production (first patented by Norrbottens Jaernverk AB in 1977 [31]), then more generally studied from a metallurgical and thermomechanical point of view [32].

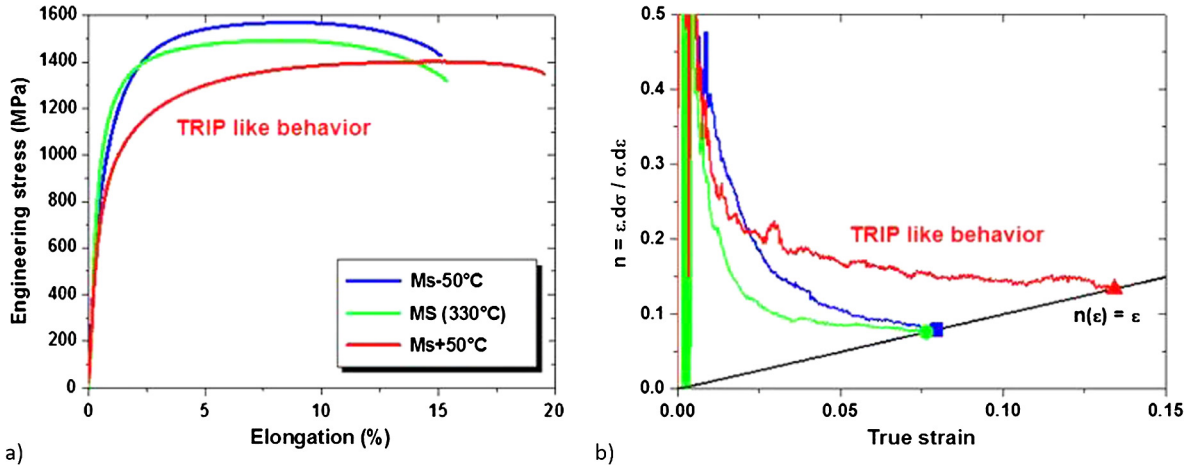

Fig. 4. Stress–strain curves (a) and evolution of the strain hardening with respect to the strain (b) for a Fe–0.3C–2.5Mn–1.5Si (in wt.%) steel tempered at different temperatures about M_s after austenitization and quenching. For temperatures equal to M_s or (M_s–50 °C), a DP-like behavior is observed, while a TRIP-like behavior is evidenced for (M + 50 °C) for which the retained austenite is still present (from [28]).

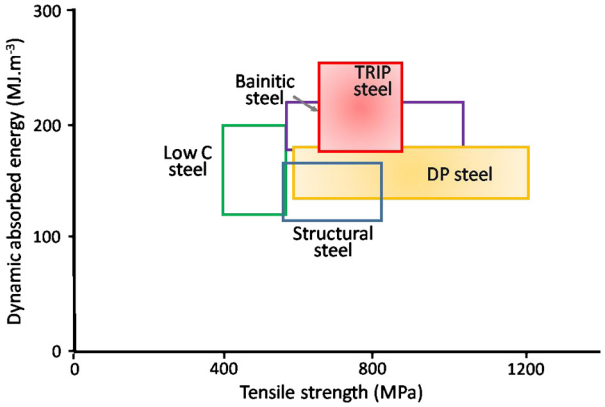

Fig. 5. Comparison of energy absorption between TRIP steels and other high-strength low-carbon steels (from [3]).

The scientific challenge for steel development was to adjust the chemical composition to have an easy formable austenite at high temperature, a quenchable steel, not too alloyed for keeping a good weldability and an acceptable cost [33]. Carbon amount is then kept low enough, and boron is added to increase the quenching ability, that is, to decrease the minimum cooling rate to transform totally austenite in martensite at room temperature. A typical grade is the 22MnB5 steel with 0.22 wt.% carbon and a few tenths of ppm boron. Additions of 1.3 wt.% manganese and 0.2 wt.% chromium are used to increase the strength of the quenched material. Copper, sulfur, and phosphorus are kept as low as possible to limit hot temperature cracking during stamping.

In the simplest direct method, the blanks are heated in the austenitic domain (usually between 900 and 950 °C), then transferred to the press. At high temperature, carbon steel is a highly formable austenite, so rather complex shapes can be stamped [34]. For example, at 800 °C, 22MnB5 grade has a yield stress of 300 MPa with a uniform elongation higher than 60% [35].

Right after stamping between 650 and 850 °C, parts are cooled down under pressure in the die, forming tools being water cooled (Fig. 6) [31]. The cooling rate is of the order of 50 to 100 K/s, enough for martensitic transformation to proceed within the whole part. The tensile strength of the final part is about 1600 MPa.[2] The total cycle time is less than 25 s, compatible with automotive part production [35]. Such a final strength is mostly used for safety parts for which a minimal deformation is expected (anti-intrusion parts as B-Pillar or bumpers). New press-hardened steels are currently developed to further improve the crash resistance and extend the range of application of such products to new parts for energy absorption.

[2] It is to be noted that a martensitic grade with a similar tensile strength is limited to 3% of uniform elongation, which prevents any stamping except bending.

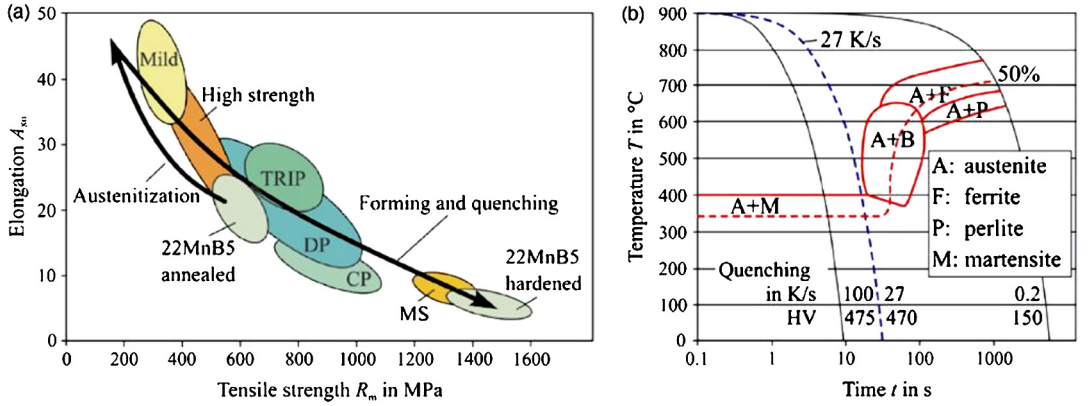

Fig. 6. Mechanical characteristics of a 22MnB5 steel and its CCT diagram [31] (© 2010, with kind permission from Elsevier).

Table 1
Stacking fault energy (SFE) for some typical C and Mn amounts of TRIP steels (from [43]).

C (wt.%)	0.6	1.2	1.2	0.95	0	0.5	1
Mn (wt.%)	22	22	12	17	30	30	30
SFE (mJ/m^2)	37	49	47	42	34	42	49

Nevertheless, a high-temperature process is not easy to manage. First, the friction coefficient between the sheet and the tools is to be controlled and the oxidation of the sheet surface limited. The sheets are then coated with a 20- to 30-µm-thick layer of aluminum–silicon before heating [36]. An aluminized boron steel (22MnB5) was then developed for automotive direct hot stamping applications [37]. This pre-coated solution was proposed to prevent scaling and decarburization during the austenitization step. During heating, iron diffuses in the coating and forms heat-resistant intermetallics [38]. Coating decreases the friction coefficient and protects the sheet surface. Moreover, the aluminum–silicon coating gives a good protection of the final part against corrosion.

The second challenge is to predict the final shape, the microstructure, and the mechanical properties of the hot stamped part, as deformation, temperature, and cooling rate are heterogeneous during the process. The steel development has been then accompanied with complex thermomechanical finite-element software including metallurgical evolutions during heating, deformation, and cooling [35,39,40].

3. High-manganese TWIP steels

3.1. Twinning mechanism in austenitic steels

It is well known from stainless steel development that crystallographic structure strongly influences work hardening by dislocations. In fact, the fcc structure, for which dislocations can interact to form sessile locks, usually leads to higher work hardening than the bcc structure, in which cross slip of screw dislocations is easy. Therefore, austenitic stainless steels have a much higher formability in expansion than ferritic grades.

When the bcc ferritic structure is the equilibrium phase for pure iron and low carbon steels at room temperature, addition of alloying elements such as nickel, cobalt or manganese favors austenite stability at low temperatures. For automotive applications for which a low price is important, manganese is used as the major alloying element. In addition to favoring austenite stability, carbon and manganese control the stacking fault energy (SFE), which determines the nature of dislocation gliding (Table 1). At low SFE values, dislocations dissociate in two partial dislocations delineating a band with a default in the crystallographic arrangement (Fig. 7a) [41,42]. This promotes planar slip with formation of Lomer–Cottrell locks, which increases strain hardening (Fig. 7b) [42].

When the SFE values range between 12 and 40 mJ/m^2 – the limiting values are slightly dependent on the study [44–47] – dislocation slip is completed by twinning (Fig. 7c) [43]. Twins propagate quickly through the grain and act as new boundaries [42,48]. This leads to a progressive decrease of the mean free path of dislocations according to a Hall–Petch-like relation, sometimes called “dynamic Hall–Petch effect” [46,49]. Based on the Mecking–Kocks approach [50], the flow stress σ is equal to:

$$\sigma = \sigma_0 + \alpha M \mu b \sqrt{\rho} \tag{4}$$

with σ_0 the friction stress, α a constant close to 0.4, M the Taylor factor, μ the shear modulus, b the Burgers vector, and ρ the dislocation density. The total plastic strain results from dislocation glide and twinning and is expressed by a mixture law [51]:

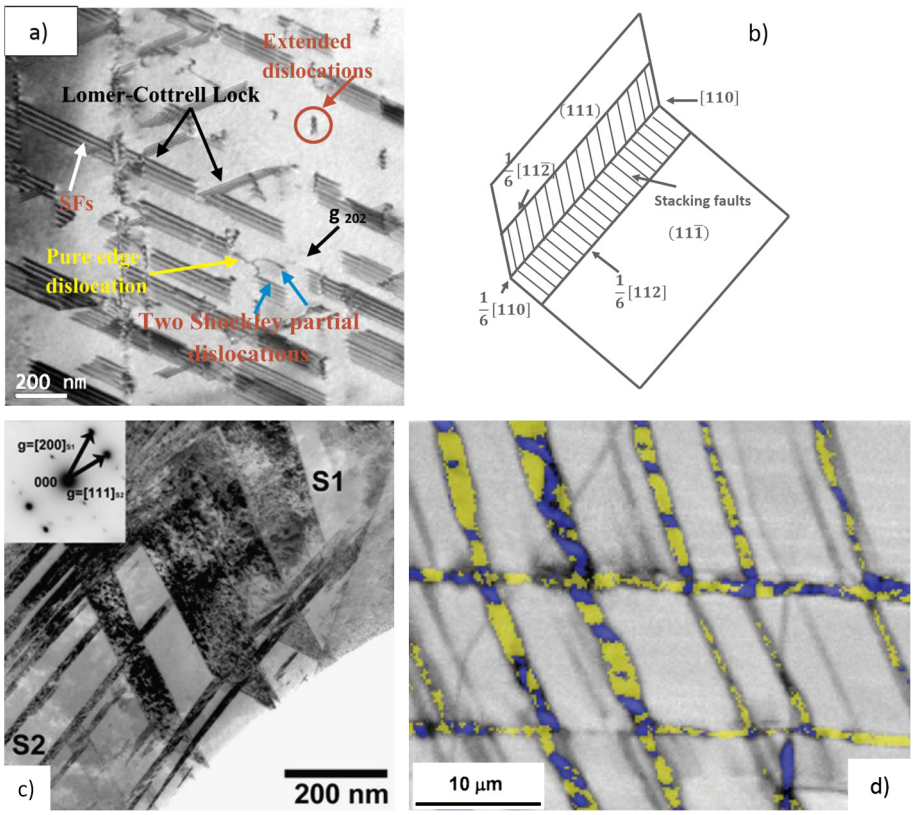

Fig. 7. Dissociated dislocations delineating a ribbon of stacking fault in an austenitic Fe–20Mn TWIP steel (a) and schematic diagram of the formation of a Lomer–Cottrell lock (b); (c) Twins in a Fe–0.6C–22Mn TWIP steel; (d) ε-martensite (in yellow) and α'-martensite (in blue) intercrossing in an austenitic Fe–16Cr–6Mn–6Ni TRIP steel. [(b) and TEM micrographs (a): [42], © 2018; (c): [43], © 2011, with kind permission from Elsevier] [(d): [41], © 2011, with kind permission from Wiley].

$$\mathrm{d}\gamma = (1-F)\mathrm{d}\gamma_g + F\mathrm{d}\gamma_t \tag{5}$$

where $\mathrm{d}\gamma_g$ is the contribution to shearing of the dislocations and $\mathrm{d}\gamma_t$ is the incremental shear due to twin formation. F is the volume fraction of twins.

The hardening comes from the evolution of the dislocation density, which is the balance between the dislocation accumulation (the inverse of the mean free path limited by the grain size d, the average distance between twins t, and the density of dislocations) and the annihilation function of ρ:

$$\frac{\mathrm{d}\rho}{\mathrm{d}\gamma_g} = \frac{1}{b}\left(\frac{1}{d}+\frac{1}{t}+k\sqrt{\rho}\right) - f\rho \tag{6}$$

t is related to the twin thickness e by the relation: $t = 2e\frac{1-F}{F}$, where F can be derived from Olson–Cohen's assumption (see Eq. (3)): $\mathrm{d}F = (1-F)m\mathrm{d}\varepsilon$. So, the twin volume fraction evolves as:

$$F = 1 - \exp(-m\varepsilon) \tag{7}$$

Combining these equations, Eq. (6) can be written:

$$\frac{\mathrm{d}\rho}{\mathrm{d}\gamma_g} = \frac{1}{b}\left(\frac{1}{d}+\frac{1}{2e}\frac{F}{1-F}+k\sqrt{\rho}\right) - f\rho \tag{8}$$

For a typical Fe–Mn–C TWIP steel, σ_0 is equal to 120 MPa, and the constants k, f and m are respectively equal to $1.1\cdot 10^{-2}$, 3, and 1.95 [49].

Beyond this dynamic Hall–Petch effect, additional hardening comes from compatibility stresses that accommodate the misfit between intra-twin and extra-twin strains within a grain (the so-called "composite effect" [52]).

For SFE lower than 10–15 mJ/m^2 at room temperature, or during straining at low temperature, austenite becomes mechanically unstable and transforms into hexagonal ε-martensite and/or quadratic α'-martensite (Fig. 7d) [41]. Even though the transition from the twinning mechanism and the induced-transformation is not totally understood as a function of the

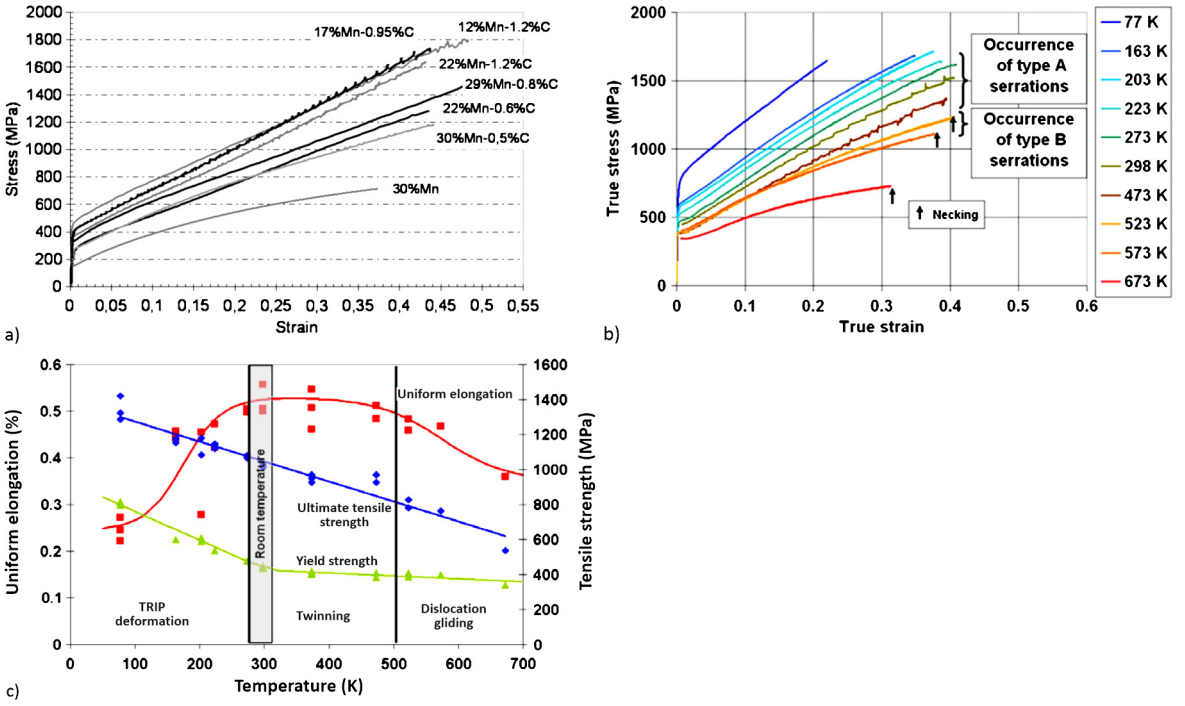

Fig. 8. Influence of the composition (a) and of the deformation temperature (b) on the stress–strain behavior of TWIP steels. Note, for some compositions and deformation temperature, the occurrence of a serrated flow mainly associated with dynamic strain aging [43] (© 2011, with kind permission from Elsevier). (c) Deformation mechanism for the optimum behavior of TWIP steels: the gray band corresponds to the best strength–elongation compromise at room temperature [53] (© 2006, with permission from EDP Sciences).

SFE value, it seems largely admitted that ε-martensite forms by combination of parallel micro-twins and α'-martensite nucleates at twins or dissociated dislocation junctions [41]. In these cases, the behavior of the steel is similar to that of an unstable austenitic stainless steel and very close to the one of a TRIP steel presented above.

3.2. Development of a second generation of high-strength steel

The behavior of high-manganese austenitic steel is very sensitive to their chemical composition, since the SFE value directly influences the deformation mechanisms (Fig. 8a) [43]. Similar effect is seen for a Fe–22wt.%Mn–0.6wt.%C–grade alloy when the straining temperature is changed (Fig. 8b) [43]. It appears that an optimum in the uniform elongation vs. UTS curve is obtained for twinning deformation in a domain close to that of the TRIP deformation (Fig. 8c) [53]. These results allow us to draw the optimum C–Mn composition in a diagram representing iso-SFE curves (Fig. 9) [46]. It should be noted that the optimum range does not correspond to a unique SFE value. This is mainly linked to the carbon effect, which is much more efficient on the twinning nucleation than on the SFE value. In this way, carbon addition has a larger influence on strain hardening than on yield stress. It was effectively shown that carbon hardens twins in these grades through an interaction between the carbon atoms and the dislocations within twins [54]. This leads to an increase in the composite effect. However, the carbon amount has to be limited, usually below 0.65–0.7 wt.%, to avoid any carbide precipitation above 700 °C.

At specific strain rates and temperatures, dynamic strain aging (DSA) is observed during tension (see, for instance, the 17%Mn–0.95%C curve in Fig. 8a or the behavior at 273 K in Fig. 8b). This is evidenced by serrated stress–strain curves and the propagation of localized deformation bands along the tensile specimen. The DSA domain depends on the alloy composition. Though not totally explained, this phenomenon seems to be linked to a strong interaction between the dislocations and the C–Mn complex [55]. It induces a rapid fracture with a limited necking and a slant fracture [56]. For practical industrial purpose, this behavior needs to be avoided. Since temperature and strain rate are most of the time imposed, some aluminum addition can limit DSA [57].

These first results led to the definition of an optimum target composition for AHSS 2nd-generation TWIP steel with 0.6 wt.% C, 22 wt.% Mn, which gives a yield stress and a UTS of 500 MPa and 1000 MPa, respectively, with a uniform elongation of 50%.

The high-Mn grades are very sensitive to the grain size [43]. The lower the grain size, the higher the yield stress and the larger the elongation at least until a grain size of 1 µm. Unlike ferritic steel grades, the effect of the grain size is larger for UTS than for yield stress. This can be explained by the twinning deformation, which induces a larger strain hardening when the grain size is smaller. Carbon was also seen to increase the Hall–Petch effect. The cold rolling and annealing conditions

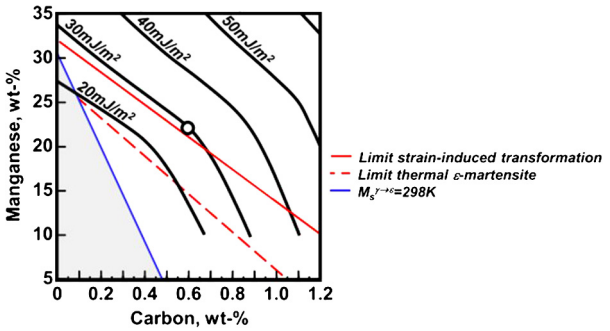

Fig. 9. Position of the optimum composition of a Fe–Mn–C TWIP steel (open circle) in a SFE diagram as a function of the C and Mn amounts (from [46]).

are then adjusted to obtain a grain size close to a micrometer. Vanadium addition is also used to refine the grain size, carbide VC particles limiting grain growth after recrystallization during annealing.

Delayed hydrogen cracking and stress corrosion cracking (SCC) were important issues for the industrial development of these grades. They were mostly circumvented by decreasing the manganese amount [58], adding vanadium for trapping hydrogen with carbides [59], or alloying with addition of aluminum and copper [60].

3.3. Industrial process challenges

Though the performance of high-Mn steels is very attractive, such an alloyed grade is not easy to produce. The ferro-manganese species that are added to reach the high amount of manganese have to be very clean to avoid any phosphor and sulfur addition. In a same way, nitrogen is to be limited to low amounts. During the high-temperature process, manganese favors internal oxidation, at the origin of surface defects; silicon can be added to limit this effect [61]. The interaction between carbon and manganese induces important segregation, which gives rise to heterogeneous microstructures, even if a recent work tends to prove that it could be useful for increasing both the strength and the elongation [62]. Finally, since there is no phase transformation from the liquid state to room temperature, the rolling and annealing temperatures have to be strictly controlled to allow a complete recrystallization during the solid-state process to limit the heredity of the texture coming from the solidification [43]. A last practical point is the management of the scraps as they are strongly alloyed compared with the usual steel shop production.

Finally, since the yield stress is relatively low and can be achieved with 1st-generation AHSSs, the potential use of such grades is for complex parts for which deformation is large enough to benefit from high strain hardening. Hydroformed pipes have been proposed as an interesting process to exploit the forming capabilities of the high-Mn 2nd-generation AHSS grades while keeping a potential to absorb energy in case of a car crash. Low commercial development has been finalized for automotive applications until now. Industrial trends are now oriented to increase the strength of high-Mn austenitic steels by limiting the manganese content (down to 12% Mn) and adjusting the carbon amount (0.4–0.9 wt.%).

4. 3rd-generation advanced high-strength steels

4.1. Metallurgy of steels with unstable austenite

A limitation of the TRIP steels described above is the low volume fraction of retained austenite that can be reached with a limited amount of carbon. It leads to moderately high UTS values and, even with a rather slow kinetics of strain-induced martensitic transformation, the contribution to strain hardening is not enough to largely increase the uniform elongation. Based on the knowledge of duplex stainless steels, it is possible to adjust the amount of retained austenite at room temperature and its stability with alloying elements as carbon, manganese, nickel… However, it directly impacts the steel's cost and can be detrimental to the welding properties. To overpass this lock, a third generation of AHSS grades is born based either on the quenching-and-partitioning process (Q&P steels) [63] or on the properties of medium-manganese steels (medium-Mn) [64,65]. In this case, the nominal composition of steel is not adequate for keeping the retained austenite at room temperature, but annealing, cooling, and thermal processes are optimized to change the austenite's composition and decrease its M_s temperature. As an example, a typical schedule for a Q&P process applied on a Fe–0.22C–1.8Mn–1.4Si (in wt.%) consists in austenizing in the intercritical domain to form a given volume fraction of austenite, then quenching to 280 °C and re-heat at 350 °C to favor C and Mn diffusion to austenite [66]. For medium-Mn steels, a larger manganese amount (typically between 5 to 8 wt.%) slightly simplifies the thermal treatment. The intercritical annealing allows one to form austenite and to increase its content in carbon and manganese; then the steel is cooled down to room temperature [67]. For both cases, the mechanical behavior takes advantage of a complex multiphase microstructure with fine grain and a TRIP effect coming from the progressive transformation of the retained austenite during straining. Typical UTS above 1200 MPa and uniform elongation larger than 12% can be achieved [26].

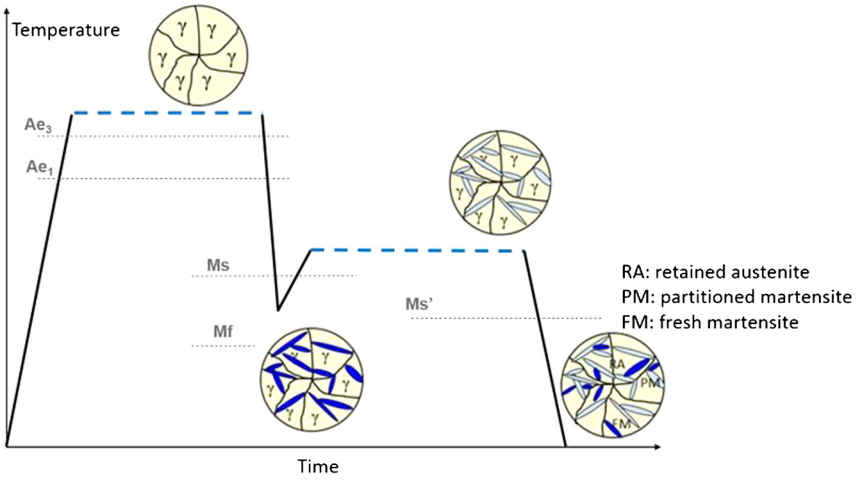

Fig. 10. Schematic representation of the thermal schedule after cold rolling and typical evolution of the multiphase microstructure.

4.2. Microstructural properties and formability of Q&P steels

The concept of Q&P process for thin sheets, firstly published by J. Speer in 2003 [63,68] is based on a quenching down to a temperature below M_s, where austenite is not fully transformed (Fig. 10). Due the alloying concept for Q&P steels – C between 0.15 and 0.4 wt.%; Mn between 1.5 and 2.5 wt.%; and (Al + Si) around 1.5 wt.% – this temperature usually lies in the range 200–350 °C. The microstructure is therefore a mixture of martensite and austenite. Steel is then reheated and aging is performed between 300 °C and 500 °C, termed "partitioning step". During this partitioning treatment, carbon diffuses from the supersaturated martensite, inducing:

- a carbon enrichment of austenite, favoring its stability at room temperature, and then promoting a further TRIP effect during straining;
- a tempering of martensite, which drastically improves its damage resistance properties, keeping a very high strength.

This simplified scheme (Fig. 10) does not reveal all the complex evolution of the microstructure during partitioning, which is at the core of fundamental metallurgical studies. The detailed mechanisms of Q&P evolution are still a matter of debate [69]. For instance, the formation of bainite during partitioning cannot be completely ruled out and could explain the measured enrichment of carbon in the retained austenite, as the partitioning temperatures are consistent with those for bainite formation [70]. For a complete characterization of Q&P microstructures, advanced techniques are used, including electron microscopy, *in-situ* X-ray diffraction or Atom Probe Tomography (Fig. 11) [71].

Even if detailed mechanisms are not yet elucidated, the benefits of such a Q&P treatment in terms of improved mechanical properties have been clearly demonstrated [63,72]. The current range of strength achievable with this new concept is between 1000 and 1500 MPa, with a total elongation reaching 20%. Moreover, as the matrix is a kind of tempered martensite, damage resistance is improved compared to DP or TRIP steels with the same strength. One of the key features of those new steels is the extreme fineness of the constituent microstructure made of laths (martensite, bainite, or retained austenite), whose characteristic size is much less than 1 µm (Fig. 11). This also contributes to increasing both the strength and the mechanical stability of austenite.

The development of such grades requires an important modification of the annealing line, for which a quenching and reheating step was not possible until recent years. The strong request from the automotive market towards 3rd-generation advanced high-strength steels has led steel making companies to invest in the upgrading of their annealing lines to ensure manufacturability of Q&P steel products.

4.3. Mechanical behavior of medium-Mn steels

Recent literature reports many works on medium-Mn steels varying their chemical composition. A largely studied composition is 0.2 wt.% C–5 wt.% Mn, where aluminum and silicon are added to limit the carbide precipitation. For such a composition, the intercritical annealing temperature lies between 740 and 780 °C. It influences strongly the mechanical behavior in tension as seen in Fig. 12 [73]. Examples of after-annealing microstructures are given in Fig. 13. Ferrite and austenite are intimately intertwined, with a fine grain size about 0.5 µm. For the highest annealing temperature (Fig. 13b) martensite is present within the austenite islands.

A first trend is the increase in strain hardening and in UTS values when the annealing temperature increases. Uniform elongation also depends on the temperature, with a maximum value for an intermediate temperature (close to 760 °C in

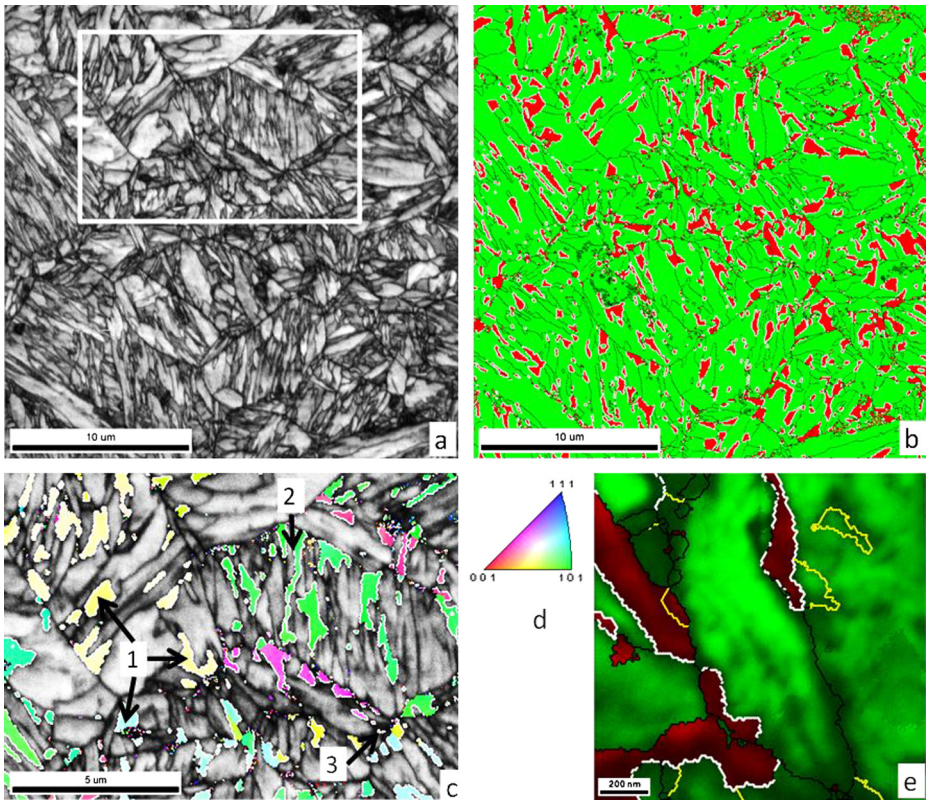

Fig. 11. High-resolution EBSD data showing different morphologies of retained austenite in a Q&P microstructure: (a) image quality (IQ) map; (b) phase distribution [red: retained austenite, green: martensite]; (c) IQ map [enlargement of the white rectangle in (a)]; (d) austenite grain orientation in (c); (e) retained austenite (in red) along martensite laths (in green) – information from transmission Kikuchi diffraction in SEM through a TEM thin foil [71], (© 2016, with kind permission from Elsevier).

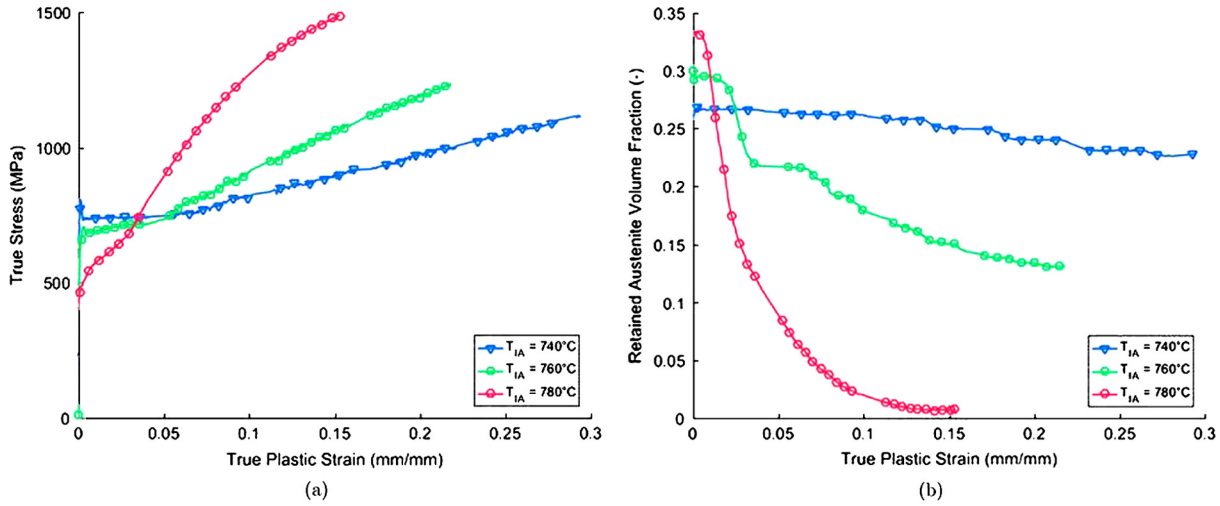

Fig. 12. Stress–strain behavior of medium-Mn steels (0.2C–5Mn–2.5Al, in wt.%) after being subjected to different intercritical annealing temperatures (a), and strain-induced evolution of the volume fraction of retained austenite (b) [73] (© 2017, with kind permission from Elsevier).

the present case, Fig. 12). During straining, the strain-induced martensite is quantified by *in-situ* magnetic measurements (Fig. 12b) [73]. The mechanical behavior results from the deformation mechanism: when the austenite is too stable at room temperature, its transformation kinetics with strain is too slow to sustain large deformation; moreover, it corresponds to a low volume fraction of austenite, thus to a moderate hardening by strain-induced martensite. On another hand, unstable austenite leads to a three-phase microstructure, ferrite–austenite–martensite, and the behavior is then close to that of a DP steel. The behavior is very sensitive to the annealing temperature – drastic changes within a range from 40 °C to about

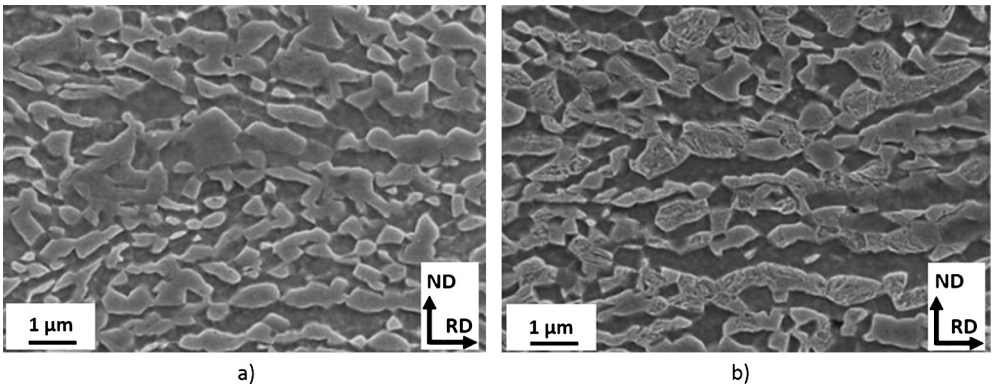

Fig. 13. Typical medium-Mn (0.2C–5Mn–2.5Al, in wt.%) microstructure after annealing at 740 °C (a) and 780 °C (b). Note the presence of martensite within the austenite islands in (b).

760 °C in the present case –, which rises difficulties for the industrial process. The annealing process robustness increases when the carbon and manganese amounts decrease, but this is detrimental to the mechanical properties, as the austenite stability and volume fraction are lower. Another way is to add aluminum: 3 wt.% aluminum increases the robustness by a factor of 3 compared to alloying with 1 wt.% aluminum [74].

Stress–strain curves exhibit Lüders and PLC-like behaviors (plateau in Fig. 12a for T_{IA} equal to 740 and 760 °C), at least for the lowest intercritical temperatures, for which no martensite is present before straining. This induces heterogeneous deformation along the tensile specimen, as it is visualized by digital image correlation [73]. Even if the martensitic transformation is not the reason for these instabilities, it is largely favored within the deformation bands. The lower the annealing temperature is, the longer the Lüders plateau. The PLC phenomenon decreases when the temperature increases and is no longer observed at high annealing temperature (e.g., 780 °C, Fig. 12a).

The mechanical behavior of the medium-Mn steels and its high sensitivity to the composition and process parameters make complex steel property optimization. To go further and speed up the developments, thermodynamic, kinetics, and mechanical models have to be developed and linked together within a reverse metallurgy process to define a priori the process parameters allowing one to obtain the targeted mechanical properties. Recent work was performed in this way, first to complete the thermodynamic data base with results for medium-Mn steels [74,75]. This was completed by atomic *ab initio* simulations to quantify the equilibrium phases at different temperatures while limiting the number of long experiments [74,76]. Linked to kinetics calculation during heating and cooling [77], the final microstructure can be predicted and the mechanical behavior estimated. Metallurgical simulations have proved themselves to be of great importance for the development and industrialization of these new steel grades.

4.4. Toward low-density medium-Mn steels

Looking for weight reduction of vehicles is in fact achieved with materials increasing the specific yield stress and/or the specific UTS. It means, for instance, that a steel grade having a UTS of 800 MPa gives rise to a part with the same mass as when using a grade with a 1000 MPa UTS if its density is 10% lower. Aluminum addition, which is commonly used to suppress cementite precipitation in austenite, can be made in much larger amounts than the usual 2 to 3 wt.%. It is accepted that adding 1 wt.% aluminum in steel decreases its density by about 1.5% [78]. Large addition of aluminum can lead to a fully ferritic steel at room temperature, so carbon and manganese have to be adjusted in consequence. In this way, an alloy with 2 wt.% aluminum, 30 wt.% manganese and 1.2 wt.% carbon is fully austenitic [79], but this kind of alloy combines the problems of the high-manganese TWIP steels with a M_3C cementite precipitation, detrimental to the elongation.

Manganese is to be limited to avoid precipitation of a κ-phase such as $(Fe,Mn)_3AlC$, which could be detrimental to ductility, while there is no definite result in the recent literature [80].

The most promising path thus derives from medium-Mn metallurgy, lowering carbon and aluminum amounts. It leads to the development of a low-density medium steel family with 0.2 to 0.5 wt.% carbon, 2 to 8 wt.% manganese, and 5 to 8 wt.% aluminum. The solidification is in the δ-ferrite domain, and the austenitic transformation is not complete during cooling so that a bimodal microstructure is obtained after cold rolling and annealing with layers of δ-ferrite with relatively large grains (a few tenths of µm) and fine grained duplex ferrite–austenite (Fig. 14). The layered microstructure can be used in fact for optimizing the mechanical properties [81], while the presence of a δ-ferrite layer suppresses the Lüders band. The yield stress is relatively high, about 600 MPa, and the strain hardening is low as the UTS is about 800 MPa. Nevertheless, the microstructure is such that a uniform elongation of about 30% can be achieved. Necking is almost absent and fracture is much localized, with a slant type [82].

The addition of aluminum increases the robustness of the industrial process and, for instance, the final properties are less dependent on the annealing temperature than medium-Mn grades with low aluminum amount. However, aluminum addition can lead to steelmaking difficulties as nozzle clogging, which make such grades challenging to produce [83].

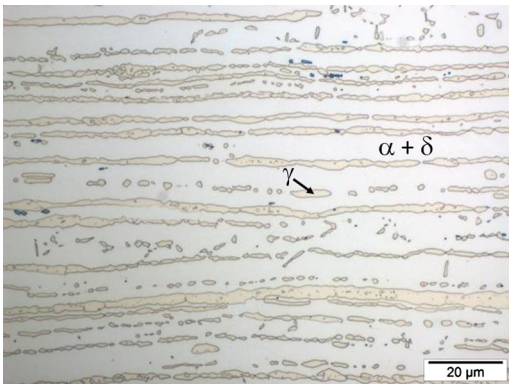

Fig. 14. Typical banded microstructure in a low-density medium-Mn medium-Al steel (0.3C–6.7Mn–6Al in wt.%). α- and δ-ferrite appear in clear gray, and austenite in light yellow (optical micrograph).

5. Conclusions and perspectives

This paper showed how the many specificities of iron alloys have been used along the past thirty years to increase the strength of steels while not impairing the ductility too much. Beyond the most conventional ferritic low-alloyed grades used by the automotive industry, several new families of advanced high-strength steels have been developed for cold-forming application, some of them being even industrialized now: the first generation of AHSS, including DP and TRIP steels, the second generation of austenitic TWIP steels, and the third generation of AHSS, which includes Q&P steels and duplex medium Mn steels. In fact, thanks to the chemical composition and a strictly controlled process, final mechanical properties take advantage of the possible co-existence of two phases – ferrite (including non-equilibrium ferritic constituents like bainite and martensite) and austenite – at room temperature, and of the potential low stability of the austenite during straining, which progressively contributes to strain hardening while deformation progresses.

The industrialization of these new grades is also strongly associated with the capabilities of the production lines, mainly the thermal treatment efficiency at relatively high speed, and with the instrumentation for quality control. Thus, it is often linked to a dedicated investment, since the right microstructure results from the alloy composition and the thermomechanical treatment.

Alloy development is also associated with the combination of different grades for a single part, adjusting material and properties only where they are mechanically needed. Taylor blanks are a good example where sheets with different thicknesses and/or different mechanical properties are laser-welded together before deep drawing. These different efforts contribute largely to a decrease in vehicle weight, since the part's thickness can be drastically reduced. Then a new limitation arises: as the sheet's thickness diminishes, the part's stiffness decreases, even if the Young's modulus of steel – between 190 and 225 GPa – is still much higher than for light alloys. The ways to improve the Young's modulus are very few, since it mostly results from the atomic interaction between iron atoms. Composites steel-TiB, for which a particle volume fraction of 10% grows the Young's modulus by 15%, or multi-materials combining steel with other materials, as sandwich panels, could be answers to this new challenge.

Finally, apart from these recent developments for automotive applications, it is to be noted many evolutions for other economic sectors as energy or aeronautic industry. New stainless grades, martensitic and duplex, emerge for their high strength and high corrosion resistance. In this way, for instance, 16 wt.% Cr–5 wt.% Ni martensitic grades with copper and niobium additions have been recently patented for aeronautic and petroleum production applications. It can be bet that synergies between these different steel applications will irrigate automotive applications forward.

To conclude, if iron is one of the most ancient metals the mankind has never been using, steel still offers many opportunities to be developed.

References

[1] E.W. Hart, Theory of the tensile test, Acta Metall. 15 (1967) 351–355.
[2] G. Cole, A. Glove, R. Jeryan, G. Davies, Steel World 2 (1997) 75–83.
[3] J. Galán, L. Samek, P. Verleysen, K. Verbeken, Y. Houbaert, Advanced high strength steels for automotive industry, Rev. Metal. 48 (2012) 118–131.
[4] G. Krauss, Martensite in steel: strength and structure, Mater. Sci. Eng. A 273 (1999) 40–57.
[5] G. Thewlis, Classification and quantification of microstructures in steels, Mater. Sci. Technol. 20 (2004) 143–160.
[6] J.Y. Koo, M.J. Young, G. Thomas, On the law of mixtures and dual phase steels, Metall. Trans. A 11 (1980) 852–854.
[7] S. Allain, O. Bouaziz, M. Takahashi, Toward a new interpretation of the mechanical behaviour of as quenched low alloyed martensitic steels, ISIJ Int. 52 (2012) 717–722.
[8] S. Van Bohemen, Bainite and martensite start temperature calculated with exponential carbon dependence, Mater. Sci. Technol. 28 (2012) 487–495.
[9] F.B. Pickering, Physical Metallurgy and Design of Steels, Applied Science Publishers, London, UK, 1978.
[10] G.B. Olson, M. Cohen, A mechanism for the strain-induced nucleation of martensitic transformations, J. Less-Common Met. 28 (1972) 107–118.
[11] G.B. Olson, M. Cohen, Kinetics of strain-induced martensitic nucleation, Metall. Trans. A 6A (1975) 791–795.

[12] V.F. Zackay, E.R. Parker, D. Fahr, R. Busch, Enhancement of ductility in high-strength steels, A.S.M. Trans. Q. 60 (1967) 252–259.
[13] J.C. Bittence, Dual-phase steels promise higher strength plus formability, Mater. Eng. 87 (1978) 39–42.
[14] C.A.N. Lanzillotto, F.B. Pickering, Structure property relationships in dual-phase steels, Met. Sci. 16 (1982) 371–382.
[15] R.A. Kot, B.L. Bramfitt (Eds.), Fundamentals of Dula-Phase Steels, TMS-AIME, New-York, 1979.
[16] B. Ghosh, O.N. Mohanty, Partitioning of micro-additions in dual-phase steels and structure property correlation, Trans. Indian Inst. Met. 49 (1996) 143–150.
[17] S.Y.P. Allain, O. Bouaziz, I. Pushkavera, C.P. Scott, Towards the microstructure design of DP steels: a generic size-sensitive mean-field mechanical model, Mater. Sci. Eng. A 637 (2015) 222–234.
[18] T. Waterschoot, B.C. De Cooman, A.K. De, S. Vandeputte, Static strain aging phenomena in cold-rolled dual-phase steels, Metall. Mater. Trans. A 34A (2003) 781–791.
[19] F.P. Pleschiutschnigg, V.V. Jamnis, S.R. Talwar, A.K. Misra, R.P.V. Atluri, R.B. Singh, P. Shankar, R.K. Verma, R.K. Goyal, V.P. Mishra, B. Deepu, P. Meierling, J. Pleschiutschnigg, Start of dual-phase hot strip production in the MPS. Dolvi plant of Ispat Industries Ltd. in India, Steel Grips 2 (2004) 171–176.
[20] A. Kyrolainen, M. Vilpas, H. Hanninen, Use of stainless steels in bus coach structures, J. Mater. Eng. Perform. 9 (2000) 669–677.
[21] S.S.M. Tavares, J.M. Pardal, M.J. Gomes da Silva, H.F.G. Abreu, M.R. da Silva, Deformation induced martensitic transformation in a 201 modified austenitic stainless steel, Mater. Charact. 60 (2009) 907–911.
[22] Y. Sakuma, D.K. Matlock, G. Krauss, Intercritically annealed and isothermally transformed 0.15 Pct C steels containing 1.2 Pct Si–1.5 Pct Mn and 4 Pct Ni: part I. Transformation, microstructure, and room-temperature mechanical properties, Metall. Trans. A 23A (1992) 1221–1232.
[23] H.K.D.H. Bhadeshia, D.V. Edmonds, Bainite transformation in a silicon steel, Metall. Trans. A 10A (1979) 895–907.
[24] P. Jacques, X. Cornet, P. Harlet, J. Ladrière, F. Delannay, Enhancement of the mechanical properties of a low-carbon, low-silicon steel by formation of a multiphased microstructure containing retained austenite, Metall. Mater. Trans. A 29A (1998) 2383–2393.
[25] D.-W. Suh, S.-J. Park, T.-H. Lee, C.-S. Oh, S.-J. Kim, Influence of Al on the microstructural evolution and mechanical behavior of low-carbon, manganese transformation-induced-plasticity steel, Metall. Mater. Trans. A 41A (2010) 397–408.
[26] O. Bouaziz, H. Zurob, M. Huang, Driving force and logic of development of advanced high strength steels for automotive applications, Steel Res. Int. 84 (2013) 937–947.
[27] G.B. Olson, M. Azrin, Transformation behavior of TRIP steels, Metall. Trans. A 9A (1978) 713–721.
[28] J.-C. Hell, M. Dehmas, S. Allain, J.M. Prado, A. Hazotte, J.-P. Chateau, Microstructure – properties relationships in carbide-free bainitic steels, ISIJ Int. 51 (2011) 1724–1732.
[29] N.C. Goel, S. Sangal, K. Tangri, A theoretical model for the flow behavior of commercial dual-phase steels containing metastable retained austenite: part I. Derivation of flow curve equations, Metall. Trans. A 16A (1985) 2013–2021.
[30] S. Sangal, N.C. Goel, K. Tangri, A theoretical model for the flow behavior of commercial dual-phase steels containing metastable retained austenite: part II. Calculation of flow curves, Metall. Trans. A 16A (1985) 2023–2029.
[31] H. Karbasian, A.E. Takkaya, A review on hot stamping, J. Mater. Process. Technol. 210 (2010) 2103–2118.
[32] M.C. Somani, L.P. Karjalainen, M. Eriksson, M. Oldenburg, Dimensional changes and microstructural evolution in a B-bearing steel in the simulated forming and quenching process, ISIJ Int. 4 (2001) 361–367.
[33] S. Cobo, T. Sturel, A. Aouafi, C. Allely, D. Cornette, Development of ultrahigh strength press hardened steel solution for structural autoparts with low sensitivity to hydrogen embrittlement, in: L. Duprez (Ed.), Proc. 3rd Int. Conf. on Metals & Hydrogen, 29–31 May 2018, Ghent, Belgium, 2018, OCAS.
[34] M. Merklein, J. Lechler, M. Geiger, Characterization of the flow properties of the quenchable ultra high strength steel 22MnB5, CIRP Ann. 55 (2006) 229–232.
[35] A. Naganathan, L. Penter, Hot stamping, in: T. Altan, A.E. Takkaya (Eds.), Steel Metal Forming – Processes and Applications, ASM Int. Pub., 2012, pp. 133–156, Ch. 7.
[36] Y.P. Jeon, Y. Se, J.D. Kim, Experimental analysis of coating layer behavior of Al–Si-coated boron steel in a hot bending process for IT applications, Int. J. Adv. Manuf. Techol. 67 (2013) 1693–1700.
[37] L. Vaissière, J.P. Laurent, A. Reinhardt, Development of pre-coated boron steel for applications on PSA Peugeot Citroën and RENAULT bodies in white, SAE Transact.: J. Mater. Manuf. 111 (2003) 909–917.
[38] Z.X. Gui, W.K. Liang, Y.S. Zhang, Enhancing ductility of the Al–Si coating on hot stamping steel by controlling the Fe–Al phase transformation during austenitization, Sci. China, Technol. Sci. 57 (2014) 1785–1793.
[39] M. Eriksson, M. Oldenburg, M.C. Somani, L.P. Karjalainen, Testing and evaluation of material data for analysis of forming and hardening of boron steel components, Model. Simul. Mater. Sci. Eng. 10 (2002) 277–294.
[40] P. Hein, A global approach of the finite element simulation of hot stamping, Adv. Mater. Res. 6–8 (2005) 763–770.
[41] D. Borisova, V. Klemm, S. Martin, S. Wolf, D. Rafaja, Microstructure defects contributing to the energy absorption in CrMnNi TRIP steels, Adv. Eng. Mater. 15 (2013) 571–582.
[42] N.K. Tewary, S.K. Ghosh, S. Chatterjee, A. Ghosh, Deformation and annealing behavior of dual phase TWIP steel from the perspective of residual stress, faults, microstructures and mechanical properties, Mater. Sci. Eng. A 733 (2018) 43–58.
[43] O. Bouaziz, S. Allain, C.P. Scott, P. Cugy, D. Barbier, High manganese austenitic twinning induced plasticity steels: a review of the microstructure properties relationships, Curr. Opin. Solid State Mater. Sci. 15 (2011) 141–168.
[44] L. Remy, A. Pineau, Twinning and Strain-induced F.C.C. → H.C.P. transformation in the Fe–Mn–Cr–C System, Mater. Sci. Eng. 28 (1977) 99–107.
[45] L. Remy, The interaction between slip and twinning systems and the influence of twinning on the mechanical behavior of fcc metals and alloys, Metall. Mater. Trans. A 12 (1981) 387–408.
[46] S. Allain, J.P. Chateau, O. Bouaziz, A physical model of the twinning-induced plasticity effect in a high manganese austenitic steel, Mater. Sci. Eng. A 387 (2004) 143–147.
[47] T.H. Lee, E. Shin, C.S. Oh, H.Y. Ha, S.J. Kim, Correlation between stacking fault energy and deformation microstructure in high-interstitial-alloyed austenitic steels, Acta Mater. 58 (2010) 3173–3186.
[48] H. Idrissi, K. Renard, L. Ryelandt, D. Shryvers, P.J. Jacques, On the mechanism of twin formation in Fe–Mn–C TWIP steels, Acta Mater. 58 (2010) 2464–2476.
[49] O. Bouaziz, N. Guelton, Modeling of TWIP effect on work-hardening, Mater. Sci. Eng. A 319 (2001) 246–249.
[50] H. Mecking, U.F. Kocks, Kinetics of flow and strain-hardening, Acta Metall. 29 (1981) 1865–1875.
[51] L. Remy, Kinetics of f.c.c. deformation twinning and its relationship to stress–strain behavior, Acta Metall. 26 (1978) 443–451.
[52] I. Gutierrez-Urrutia, D. Raabe, Dislocation and twin substructure evolution during strain hardening of an Fe–22wt.%Mn–0.6wt.%C TWIP steel observed by electron channeling contrast imaging, Acta Mater. 59 (2011) 6449–6462.
[53] C. Scott, S. Allain, M. Faral, N. Guelton, The development of a new Fe–Mn–C austenitic steel for automotive applications, Rev. Metall. CIT 103 (2006) 293–302.
[54] H. Idrissi, K. Renard, D. Schryvers, P.J. Jacques, On the relationship between the twin internal structure and the work-hardening rate of TWIP steels, Scr. Mater. 63 (2010) 961–964.
[55] S.-J. Lee, J. Kim, S.N. Kane, B.C. De Cooman, On the origin of dynamic strain aging in twinning-induced plasticity steels, Acta Mater. 59 (2011) 6809–6819.

[56] J. Lorthios, M. Mazière, X. Lemoine, P. Cugy, J. Besson, A-F. Gourgues-Lorenzon, Fracture behaviour of a Fe–22Mn–0.6C–0.2V austenitic TWIP steel, Int. J. Mech. Solids 101–102 (2015) 99–113.
[57] T.S. Shun, C.M. Wan, J.G. Byrne, A study of work-hardening in austenitic Fe–Me–C and Fe–Me–Al–C alloys, Acta Metall. Mater. 40 (1992) 3407–3412.
[58] B. De Cooman, O. Kwon, K.-G. Chin, State-of-the-knowledge on TWIP steels, Mater. Sci. Technol. 28 (2012) 513–527.
[59] B. Malard, B. Remy, C.P. Scott, A. Deschamps, J. Chêne, T. Dieudonné, M.H. Mathon, Hydrogen trapping by VC precipitates and structural defects in a high strength Fe–Mn–C steel studied by Small-Angle Neutron Scattering, Mat. Sci. Eng. A 536 (2012) 110–116.
[60] T. Dieudonne, L. Marchetti, M. Wery, J. Chene, C. Allely, P. Cugy, C.P. Scott, Role of copper and aluminum additions on the hydrogen embrittlement susceptibility of austenitic Fe–Mn–C TWIP steels, Corros. Sci. 82 (2014) 218–226.
[61] Y.F. Gong, B.C. De Cooman, Selective oxidation and sub-surface phase transformation of TWIP steel during continuous annealing, Steel Res. Int. 82 (2011) 1310–1318.
[62] M.C. Jo, H. Lee, A. Zargaran, J.H. Ryu, S.S. Soh, N.J. Kim, S. Lee, Exceptional combination of ultra-high strength and excellent ductility by inevitably generated Mn-segregation in austenitic steel, Mater. Sci. Eng. A 737 (2018) 69–76.
[63] J.G. Speer, D.V. Edmonds, F.C. Rizzo, D.K. Matlock, Partitioning of carbon from supersaturated plates of ferrite, with application to steel processing and fundamentals of the bainite transformation, Curr. Opin. Solid State Mater. Sci. 8 (2004) 219–237.
[64] R.L. Miller, Ultrafine-grained microstructures and mechanical properties of alloy-steels, Metall. Trans. 3 (1972) 905–912.
[65] A. Arlazarov, M. Gouné, O. Bouaziz, A. Hazotte, G. Petitgand, P. Barges, Evolution of microstructure and mechanical properties of medium Mn steels during double annealing, Mater. Sci. Eng. A 542 (2012) 31–39.
[66] X.C. Xiong, B. Chen, M.X. Huang, J.F. Wang, L. Wang, The effect of morphology on the stability of retained austenite in a quenched and partitioned steel, Scr. Mater. 68 (2013) 321–324.
[67] H. Luo, J. Shi, C. Wang, W. Cao, X. Sun, H. Dong, Experimental and numerical analysis on formation of stable austenite during the intercritical annealing of 5Mn steel, Acta Mater. 59 (2011) 4002–4014.
[68] J. Speer, D.H. Matlock, B.C. De Cooman, J.G. Schroth, Carbon partitioning into austenite after martensite transformation, Acta Mater. 51 (2003) 2611–2622.
[69] S.Y.P. Allain, G. Geandier, J.C. Hell, M. Soler, F. Danoix, M. Gouné, *In-situ* investigation of quenching and partitioning by high energy X-ray diffraction experiments, Scr. Mater. 131 (2017) 15–18.
[70] A.J. Clarke, J.G. Speer, M.K. Miller, R.E. Hackenberg, D.V. Edmonds, D.H. Matlock, F.C. Rizzo, K.D. Clarke, E. De Moor, Carbon partitioning to austenite from martensite or bainite during the quench and partition (Q&P) process: a critical assessment, Acta Mater. 56 (2008) 16–22.
[71] I. de Diego-Calderón, I. Sabirov, J.M. Molina-Aldareguia, C. Föjer, R. Thiessen, R.H. Petrov, Microstructural design in quenched and partitioned (Q&P) steels to improve their fracture properties, Mater. Sci. Eng. A 657 (2016) 136–146.
[72] F. Hu, K.M. Wu, Nanostructured high-carbon dual-phase steels, Scr. Mater. 65 (2011) 351–354.
[73] M. Callahan, O. Hubert, F. Hild, A. Perlade, J.-H. Schmitt, Coincidence of strain-induced TRIP and propagative PLC bands in medium Mn steels, Mater. Sci. Eng. A 704 (2017) 391–400.
[74] A. Perlade, A. Antoni, R. Besson, D. Caillard, M. Callahan, J. Emo, A.-F. Gourgues, P. Maugis, A. Mestrallet, L. Thuinet, Q. Tonizzo, J.-H. Schmitt, Development of 3rd generation Medium Mn duplex steels for automotive applications, Mater. Sci. Technol. (2018), https://doi.org/10.1080/02670836.2018.1549303, in press.
[75] A. Mestrallet, Thermodynamique de nouvelles solutions d'aciers de 3^{e} génération à structure duplex [Thermodynamics of new solutions for 3rd generation steels with a duplex microstructure], PhD thesis, Université Grenoble Alpes, Grenoble, France, 2017, https://tel.archives-ouvertes.fr/tel-01819772 (in French).
[76] J. Dequeker, Modélisation à l'échelle atomique du système Fe–Al–Mn–C à l'aide de modèles de paires et de calculs thermodynamiques (Atomistic modeling of the Fe–Al–Mn–C system using pairs model and thermodynamic calculations), Université de Lille, Lille, France, 2018.
[77] J. Emo, P. Maugis, A. Perlade, Austenite growth and stability in medium Mn, medium Al Fe–C–Mn–Al steels, Compos. Mater. Sci. 125 (2016) 206–217.
[78] G. Frommeyer, U. Brüx, Microstructures and mechanical properties of high-strength Fe–Mn–Al–C light-weight TRIPLEX steels, Steel Res. Int. 77 (2006) 627–633.
[79] I. Gutierrez-Urrutia, D. Raabe, Influence of Al content and precipitation state on the mechanical behavior of austenitic high-Mn low-density steels, Scr. Mater. 68 (2013) 343–347.
[80] H. Kim, D.W. Suh, N.J. Kim, Fe–Al–Mn–C lightweight structural alloys: a review on the microstructures and mechanical properties, Sci. Technol. Adv. Mater. 14 (2013) 014205.
[81] Y. Brechet, J.D. Embury, Architectured materials: expanding materials space, Scr. Mater. 68 (2013) 1–3.
[82] Q. Tonizzo, A.F. Gourgues-Lorenzon, M. Maziere, A. Perlade, I. Zuazo, Microstructure, plastic flow and fracture behavior of ferrite–austenite duplex low density medium Mn steel, Mater. Sci. Eng. A 706 (2017) 217–226.
[83] Y. Vermeulen, B. Coletti, B. Blanpain, P. Wollants, J. Vleugels, Material evaluation to prevent nozzle clogging during continuous casting of Al killed steels, ISIJ Int. 42 (2002) 1234–1240.